



Impacts of multiple climate factors and vegetation changes on evapotranspiration in southwest China from 1982 to 2018

Yanjun Wang ^{a,b}, Xiaorong Huang ^{a,b,*}, Yi Ao ^{a,b}

^a State Key Laboratory of Hydraulics and Mountain River Engineering, Sichuan University, Chengdu, 610065, China

^b College of Water Resource & Hydropower, Sichuan University, Chengdu, 610065, China

HIGHLIGHTS

- Decoding long-term ET changes in heterogeneous Southwest China.
- Complex Climate-Vegetation Interactions Driving ET Variability.
- Addressing Multicollinearity in Multi-Factor Analyses.
- Utilization of Remote Sensing Data for Large-Scale ET Monitoring.
- Disentangling climate and vegetation influences in karst regions.

ARTICLE INFO

Keywords:

ET
Climate change
LAI
Driving factors
Southwest China

ABSTRACT

Evapotranspiration (ET), as an essential element of the global water cycle, serves as a crucial connection for the transfer of water, carbon, and energy between the land biosphere and the atmosphere. This research concentrated on the dynamic variations in ET over 1982–2018 in Southwest China (SWC), investigating the driving mechanisms behind ET changes, particularly climate variability and vegetation dynamics. We selected long-term remote sensing and reanalysis datasets to evaluate ET dynamics in SWC. After validation against eddy covariance observations, the GLASS ET dataset with the highest accuracy was chosen for further analysis. The spatial patterns of ET across SWC and its various geomorphological subdivisions were analyzed. Overall, ET exhibited a north-to-south increasing trend, with more than 80 % of the areas in each geomorphological subdivision showing a significant upward trend in ET. Subsequently, ridge regression was employed to analyze the relative contributions of temperature (T), solar radiation (Rs), specific humidity (H), precipitation (P), wind speed (U), and leaf area index (LAI) to ET variability. T and H were found to be the dominant factors influencing ET changes, with their relative contributions exceeding 20 % during both study periods (1982–1999 and 2000–2018). Furthermore, the dominant drivers of ET changes exhibited phase-dependent variations across different geomorphological subdivisions. Additionally, the relative contribution of vegetation factors (LAI) to ET increased across all subregions. Ridge regression effectively addressed the multicollinearity issue among environmental factors, offering greater stability compared to traditional multiple linear regression. Finally, a double-log elasticity model was used to further quantify and validate the effects of different driving factors on ET, enhancing the credibility of the results. The elasticity coefficient for T was the highest and positive, while the elasticity coefficient for H was the highest and negative. These findings enhance the understanding of ET change mechanisms in SWC and are essential for elucidating regional vegetation-hydrology-climate interactions.

1. Introduction

ET is a key component of the water cycle and essential for water resource management. As a core process linking the atmosphere, soil,

and vegetation systems, it directly influences water availability, agricultural productivity, and ecosystem stability (Pereira et al., 2015; Zhu et al., 2014). Currently, global warming is intensifying the water cycle. As a key component of terrestrial water fluxes, ET plays an important

* Corresponding author. E-mail addresses: wujun@stu.scu.edu.cn (Y. Wang), hxiaorong@scu.edu.cn (X. Huang), 2024323060017@stu.scu.edu.cn (Y. Ao).

role in this process by accelerating surface water loss, enhancing land-atmosphere moisture exchange, and influencing regional precipitation patterns. It not only affects the distribution of water resources but also regulates microclimatic conditions, generating feedback effects on the climate system. Therefore, monitoring and understanding *ET* dynamics are essential for optimizing water allocation and ensuring effective ecosystem management (Sun et al., 2018; Wei et al., 2022; Yin et al., 2022). Nevertheless, as global warming intensifies and regional extreme events become more frequent and severe, the climatic and vegetation changes affecting *ET* processes have grown increasingly complex. Consequently, *ET* variability remains a highly uncertain aspect of the water cycle (Fisher et al., 2017; Liu et al., 2021; Wang et al., 2022b; Yan et al., 2013; Zhang et al., 2016b). In addition to climatic and biophysical drivers, recent studies have highlighted the growing role of human activities—such as land use change, ecological restoration, and water resource development—in shaping *ET* dynamics across various regions (Cai et al., 2022; Li et al., 2024; Wang et al., 2021a). These anthropogenic drivers may alter vegetation composition, soil moisture, and water availability, further complicating *ET* feedback mechanisms under changing climates. Thus, a systematic investigation of *ET*'s spatiotemporal variations and driving mechanisms is crucial for understanding water dynamics and supporting ecological conservation and water management under climate change (Zhang et al., 2022).

Previous studies on *ET* dynamics have primarily examined the unidirectional relationships between individual factors within the climate-vegetation-evapotranspiration system. Climate variables directly regulate *ET* by affecting atmospheric vapor pressure, soil moisture, and temperature (Li et al., 2022), while vegetation impacts the water transport and transformation processes through its *LAI*, root distribution, and growth status (Bai et al., 2020). Traditional studies often assume that these factors operate independently, holding other variables constant (Hao et al., 2018). However, this simplified approach overlooks the interactive relationship between climate and vegetation (Zhao et al., 2022). Climate change affects *ET* both directly and indirectly by modifying vegetation types and growth cycles. For instance, rising temperatures and shifting precipitation patterns can lead to vegetation changes in certain regions, thereby altering *ET* processes (Zhao and Running, 2010). Moreover, vegetation types differ substantially in their physiological structures and water-use strategies. Forests, grasslands, croplands, and shrublands exhibit distinct *ET* responses to climate variability due to differences in canopy structure, root depth, and phenological dynamics (Fu et al., 2023; Jongen et al., 2024). Ignoring vegetation-type heterogeneity may thus oversimplify the ecological interpretation of *ET* responses. Therefore, analyzing a single factor may not fully reveal the driving mechanisms behind *ET* changes, especially in complex environments where the interplay between climate and vegetation is pronounced.

Multiple studies have investigated the influence of climate and vegetation factors on *ET* dynamics. Early research often focused on specific ecosystems, watersheds, or experimental sites, where high-resolution field observations and experimental analyses were conducted to reveal the dynamic changes in *ET* and the local driving factors within particular environments (Geng et al., 2022; Tao et al., 2006). Although such studies provide relatively reliable data, they require long-term field observations. Satellite remote sensing data, on the other hand, can cover vast geographical areas and offer long-term, continuous observation records. This makes it particularly valuable for remote areas or regions where field observations are challenging. As a result, satellite remote sensing has become essential for large-scale studies due to its distinct advantages. A growing number of studies employ process-based models to assess the regional impacts of climate and vegetation changes on *ET* (Ren et al., 2024). However, in multi-factor driving analyses, multicollinearity among variables is a key issue that requires attention. Variables such as temperature, solar radiation, and precipitation often exhibit high correlations in both time and space, which may obscure the true contribution of individual factors. To tackle this issue, multiple

linear regression has been employed to analyze variables and mitigate multicollinearity (Fang et al., 2020; Pei et al., 2017; Xie et al., 2020; Yu et al., 2020).

In China, many studies have examined *ET* dynamics in regions such as the Loess Plateau and the Tibetan Plateau, yet SWC—a region characterized by karst topography, complex vegetation mosaics, and significant ecological engineering—remains underrepresented in long-term, multi-factor *ET* assessments (Zhang et al., 2021, 2023b). This region is not only a vital ecological barrier but also the upstream source of major river basins like the Yangtze and Pearl Rivers. However, limitations in field observation data, the lack of non-forest flux tower coverage, and challenges in disentangling climate, vegetation, and anthropogenic impacts have constrained our understanding of *ET* variability in SWC. In addition, many existing studies use leaf area index (*LAI*) as a vegetation proxy without accounting for differences among vegetation types, and few studies incorporate explicit human activity variables such as land use change or water infrastructure. Moreover, little is known about how future climate and land use scenarios may affect *ET* trends in the region. Therefore, this study aims to fill these gaps by integrating multi-source remote sensing and reanalysis data to explore historical *ET* dynamics and quantify the relative contributions of climate and vegetation factors using ridge regression and elasticity modeling. Therefore, it is essential to conduct multi-temporal and multi-spatial scale studies on *ET* dynamics and attribution in SWC. Therefore, to address the aforementioned gaps, this study overcomes the challenge of limited field data in SWC by utilizing extensive satellite-derived data and reanalysis datasets. These resources offer high spatial resolution and long-term consistent data, enabling the study of hydrological cycle changes and providing valuable insights for previously unmonitored regions (Sheffield et al., 2018). A ridge regression model is applied in this study to quantify the contributions of climate and vegetation factors to *ET* changes. Ridge regression is particularly suitable because it effectively handles multicollinearity among predictor variables by introducing a regularization term that shrinks coefficient estimates, thereby reducing variance and improving model stability (Walker and Birch, 1988). This approach allows more reliable attribution of *ET* variability in the presence of correlated climate and vegetation factors. Additionally, a double-log elasticity model is used to further validate the results, enhancing their robustness and persuasiveness.

From the above, this study aims to: (1) validate *ET* remote sensing products using eddy covariance-based *ET* observations, (2) examine the temporal and spatial trends of *ET*, key climate variables (temperature, solar radiation, specific humidity, precipitation, and wind speed), and vegetation over past decades, (3) assess the contributions of climate and vegetation to long-term *ET* changes, and (4) quantify the impacts of climate and vegetation changes on *ET*.

2. Materials and methods

2.1. Study area

SWC (96.64°E~112.88°E, 20.94°N~34.32°N) covers about $1.38 \times 10^6 \text{ km}^2$, accounting for 14.34 % of China's total land area (Fig. 1). It is comprised of Sichuan Province, Chongqing Municipality, Yunnan Province, Guizhou Province and Guangxi Zhuang Autonomous Region. Its complex topography of Hengduan Mountains (HDM), Ruergai Plateau (RGP), Sichuan Basin (SCB), Yunnan-Guizhou Plateau (YGP) and Guangxi Hills (GXH) is structured with elevations ranging from -100m to 6511m. The climate in SWC is predominantly tropical and subtropical monsoon, characterized by favorable water-heat conditions. Precipitation and temperature follow a spatial pattern, decreasing from southeast to northwest. The terrain decreases in steps from west to east, and the region is renowned for its complex karst topography. Among the ten major ecological security barriers such as "Two Screens and Three Belts" in China, SWC holds a vital ecological role as the source region of the Pearl River's main and tributary streams (Ying et al., 2022).

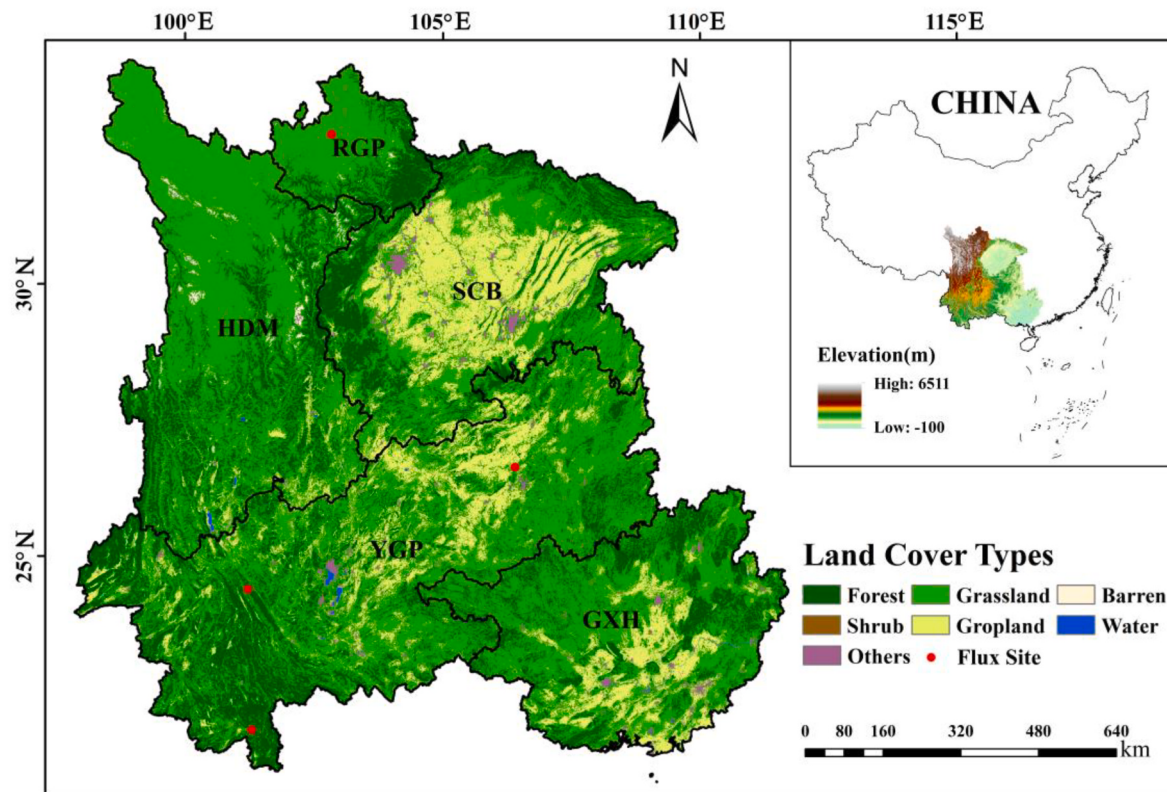


Fig. 1. The land cover types and sub-regions of Southwest China (SWC) as well as the flux sites.

However, the region's fragile karst environment (Lu et al., 2024; Zhang et al., 2024), combined with human activities, has led to challenges such as rocky desertification and soil erosion, making it highly sensitive to global environmental change (Shi et al., 2020).

2.2. Data

2.2.1. ET data

The study used four long-term ET products (Table 1), including: (1) the Global Land Evaporation Amsterdam Model (GLEAM), which provides global coverage with a spatial resolution of 0.25° and spans from 1980 to 2022 (<http://www.gleam.eu>); (2) the Famine Early Warning Systems Network Land Data Assimilation System (FLDAS), which uses meteorological datasets (e.g., TerraClimate and reanalysis datasets) as inputs. This ET product spans from 1982 onward, with a spatial resolution of 0.1° , and is provided by NASA (<http://disc.gsfc.nasa.gov>); (3) the Global Land Surface Satellite (GLASS), which offers highly accurate ET products with a spatial resolution of 0.05° . It uses a hybrid algorithm

powered by meteorological data, satellite remote sensing data, and ground-based observations, with data available from 1982 to 2018 (<http://glass.hku.hk>); (4) the Modern Era Retrospective Analysis for Research and Applications (MERRA), whose ET product combines numerical weather models with satellite data for reanalysis estimates. It has a spatial resolution of $0.5^\circ \times 0.625^\circ$ and provides data from 1980 to the present (<http://goldsmr4.gesdisc.eosdis.nasa.gov>).

2.2.2. Flux observation data

Data from four flux observation stations in China, obtained from National Ecosystem Science Data Center, were used to validate the ET products (<http://www.nesdc.org.cn>). Table 2 presents descriptions of the four flux observation stations.

The Xishuangbanna station (XSBN) is located within a tropical seasonal rainforest ecosystem. Situated at a relatively high elevation, the station experiences a lower annual average temperature and rainfall, with distinct seasonal variations in precipitation. Continuous observational data collection at this station began at the end of 2002. The Ailao Mountain station (ALM) is located within a subtropical evergreen broadleaf forest ecosystem. According to the long-term monitoring data from ALM Station, the annual average rainfall is 1931 mm. Under the influence of the southwest monsoon, the annual average temperature is 11.3°C (Qi et al., 2021a). The area is characterized by a rich diversity of plant species and community types. The flux tower at this station was officially put into operation at the end of 2008. The Puding Station (PD) joined the Chinese Ecosystem Research Network (CERN) in 2014. The area is characterized by a subtropical monsoon moist climate. During the observation period, the plot was in the early stage of natural recovery, showing significant vegetation restoration and high coverage, and can be considered an Arbor-Shrub-Grassland ecosystem. The Ruoergai Station (RG) is located within an alpine meadow ecosystem on the eastern edge of the Qinghai-Tibet Plateau. The seasons are not distinct, with a cool climate, a long winter and no summer, and short spring and autumn seasons. This station was established in May 2015.

Table 1

Descriptions of the four selected ET products.

ET Products	Generation Methods	Temporal Resolution	Spatial Resolution	Time Span	References
GLEAM	Priestley-Taylor method	Daily	$0.25^\circ \times 0.25^\circ$	1980–2023	Miralles et al. (2011)
FLDAS	Land surface method	Monthly	$0.1^\circ \times 0.1^\circ$	1982–present	McNally (2018)
GLASS	Bayesian average method	8-day	$0.05^\circ \times 0.05^\circ$	1982–2018	Yao et al. (2014)
MERRA	Reanalysis method	Monthly	$0.5^\circ \times 0.625^\circ$	1980–present	Reichle et al. (2011)

Table 2

Descriptions of the four flux observation stations.

Station	Observation Period	Location	Elevation	Ecosystem Types	References
Xishuangbanna(XSBN)	2003–2010	101.27°E 21.93°N	750m	Forest	Qi et al. (2021b)
Ailao mountain (ALM)	2009–2013	101.03°E 24.54°N	2476m	Forest	Qi et al. (2021a)
Ruoergai (RG)	2015–2018	105.22°E 32.80°N	3500m	Grassland	Chen et al. (2023)
Puding (PD)	2015–2018	106.32°E 26.60°N	1170m	Arbor-Shrub-Grassland	Wang et al. (2023)

2.2.3. Climate and vegetation data

Climate data were drawn from the China Meteorological Forcing Dataset (CMFD) (<http://data.tpdc.ac.cn>), with a spatial resolution of 0.1° and a time span from 1978 to 2018. The CMFD is generated from GLDAS by integrating remote sensing, radar data, and ground-based observations. Its accuracy lies between that of satellite remote sensing data and meteorological station observations, surpassing the precision of existing international reanalysis datasets. Five climate variables include temperature (T), downward solar radiation (Rs), specific humidity (H), precipitation (P), and wind speed (U) were used to assess their impact on ET changes.

The LAI product was obtained from GLASS as vegetation data to explain the variability in ET (<http://glass.hku.hk>). The GLASS LAI product utilizes Generalized Regression Neural Networks (GRNNs) to extract LAI from time-series AVHRR surface reflectance data. The algorithm trains GRNNs on preprocessed AVHRR reflectance data and applies a rolling processing approach to generate a temporally continuous long-series GLASS LAI product. In this study, the latest GLASS AVHRR LAI product (V50) was used, featuring a spatial resolution of 0.05° and covering the period from 1981 to 2018.

To maintain spatial and temporal consistency, all four ET products were resampled to 0.05°, and the data series was selected from 1982 to 2018.

2.3. Trend analysis

This study first analyzes the spatial distribution, change trends, and associated climate and vegetation variations of multi-year average ET in SWC from 1982 to 2018. We used the non-parametric Theil-Sen slope method to analyze long-term trends. This method offers greater accuracy than traditional linear regression when handling skewed data (Sen, 1968). In addition, to assess the significance of the trends in ET and climate variables, this study applied the non-parametric Mann-Kendall test (Kendall, 1990; Mann, 1945). The Mann-Kendall test is widely applied to evaluate the significance of long-term trends, offering robust support for climate and hydrological analyses (Shan et al., 2015).

2.4. Attribution analysis

The contributions of various driving factors to ET trends are quantified using multiple linear regression. The model is formulated as follows:

$$Y = X\omega + \varepsilon \quad (1)$$

where Y is the dependent variable; X is the independent variable; ε is the error term; ω is the regression coefficient and calculated by Ordinary Least Squares (OLS) method:

$$\omega_{OLS} = (X^T X)^{-1} X^T Y \quad (2)$$

However, when there is a strong correlation between the variables, it can lead to instability in the results of traditional regression models. Ridge regression is a method designed to address linear regression problems, particularly when the independent variables exhibit multicollinearity. Its core idea is to add a regularization term to the least squares regression, which helps to reduce model overfitting. This regularization term constrains the magnitude of the regression coefficients,

thereby decreasing the model's sensitivity to outliers (Walker and Birch, 1988):

$$\omega_{ridge} = (X^T X + \lambda I)^{-1} X^T Y \quad (3)$$

where λ is the regularization parameter; I is the identity matrix.

In this study, to explore the relationship between ecological vulnerability and various driving factors, we adopted the ridge regression model for analysis, as it offers stable estimates in the presence of multicollinearity among explanatory variables.

Firstly, the data in each group were normalized to eliminate the influence of different feature dimensions:

$$X_m = \frac{X - X_{min}}{X_{max} - X_{min}} \quad (4)$$

where X_m is the normalized value, X_{max} is the maximum value, X_{min} is the minimum value.

Then, ridge regression was performed to model the relationship between ET and the independent variables:

$$Y_m = \sum_{i=1}^n A_i X_{im} + B \quad (5)$$

where Y_m is the normalized ET ; X_{im} are the normalized independent variables; A_i are the ridge regression coefficients.

Finally, the relative contribution of different driving factors to ET were formulated:

$$\eta_{c1} = A_1 \times X_{1m_trend} \quad (6)$$

$$\eta_{rc1} = \frac{|\eta_{c1}|}{|\eta_{c1}| + |\eta_{c2}| + |\eta_{c3}| + \dots} \times 100\% \quad (7)$$

where η_{c1} is the contributions of different driving factors to the normalized ET ; X_{1m_trend} is the trend of normalized driving factor.

In this study, the regularization parameter λ was not fixed but adaptively selected for each pixel. Specifically, λ was dynamically determined by evaluating model performance over a range of candidate values (from 1 to 10 with a step size of 0.1), and selecting the value that minimized the prediction error. This approach helps improve local model stability and ensures robust regression estimates across spatially heterogeneous conditions.

2.5. Quantitative analysis

The elasticity model is used to evaluate the proportional response of a dependent variable to changes in independent variables, effectively capturing the relative rate of change between them (Ahiablame et al., 2017; Tan et al., 2020). The elasticity concept, characterized by clear physical significance and a simple formula, serves as an effective hydrological tool for analyzing the impact of climate and other factors on hydrological variables like runoff (Chen et al., 2022; Sankarasubramanian et al., 2001). Common elasticity models include the Least Square Elasticity (LSE) model, the Double Logarithm Elasticity (DLE) model, the Semi-logarithm Elasticity (SLE) model, and the Generalized Linear Elasticity (GLE) model (Tsai, 2017; Zheng et al., 2009). Unlike other elasticity models, the DLE model applies a logarithmic transformation, which not only maintains the simplicity and interpretability

of the model but also enhances its ability to fit complex nonlinear relationships. This makes it particularly useful for handling data with high correlations or significant distribution differences (Tsai, 2017). Therefore, in this study, the DLE model measured the relative contributions of climate and vegetation variability to *ET* changes. The multivariable function representing the impact of various driving factors on *ET* is formulated as follows:

$$ET = f(X) \quad (8)$$

The equation is then revised following the approach proposed by Tsai (2017) as follows:

$$ET = X^{\beta_i} \quad (9)$$

Applying the logarithm of both sides yields the following equation:

$$\log ET = \beta_i \log X \quad (10)$$

Where β_i is the elasticity coefficient of each variable. It represents the percentage change in the dependent variable Y for a 1 % increase in the independent variable X. For example, $\beta = 0.5$ means that when X increases by 1 %, Y is expected to increase by 0.5 %.

3. Results

3.1. ET products validation

To ensure the high quality of the *ET* dataset, the four *ET* products (GLEAM, FLDAS, GLASS, MERRA) were individually validated by comparing the daily flux data from the XSBN, ALS, RG and PD stations (Fig. 2). The results indicate that the GLASS *ET* product consistently demonstrates the highest agreement with observed *ET* compared to GLEAM, FLDAS, and MERRA products. This is evidenced by its highest coefficients of determination (R^2) values at every single site and its lowest root mean square errors (RMSE) at three of the four stations. Additionally, the GLEAM product also performed exceptionally well, showing a strong correlation and achieving the lowest RMSE among all products at the PD station. In contrast, the FLDAS and MERRA products showed lower accuracy, with MERRA exhibiting the worst at the XSBN station, which may be attributed to its lower spatial resolution ($0.5^\circ \times 0.67^\circ$). Overall, the GLASS product demonstrated higher reliability than GLEAM, FLDAS, and MERRA. Therefore, the subsequent analysis was conducted using GLASS-derived *ET* data. (see Sections 3.2–3.5 for details).

3.2. Spatial patterns and trends of *ET*

Fig. 3 presents the spatial distribution and statistical characteristics

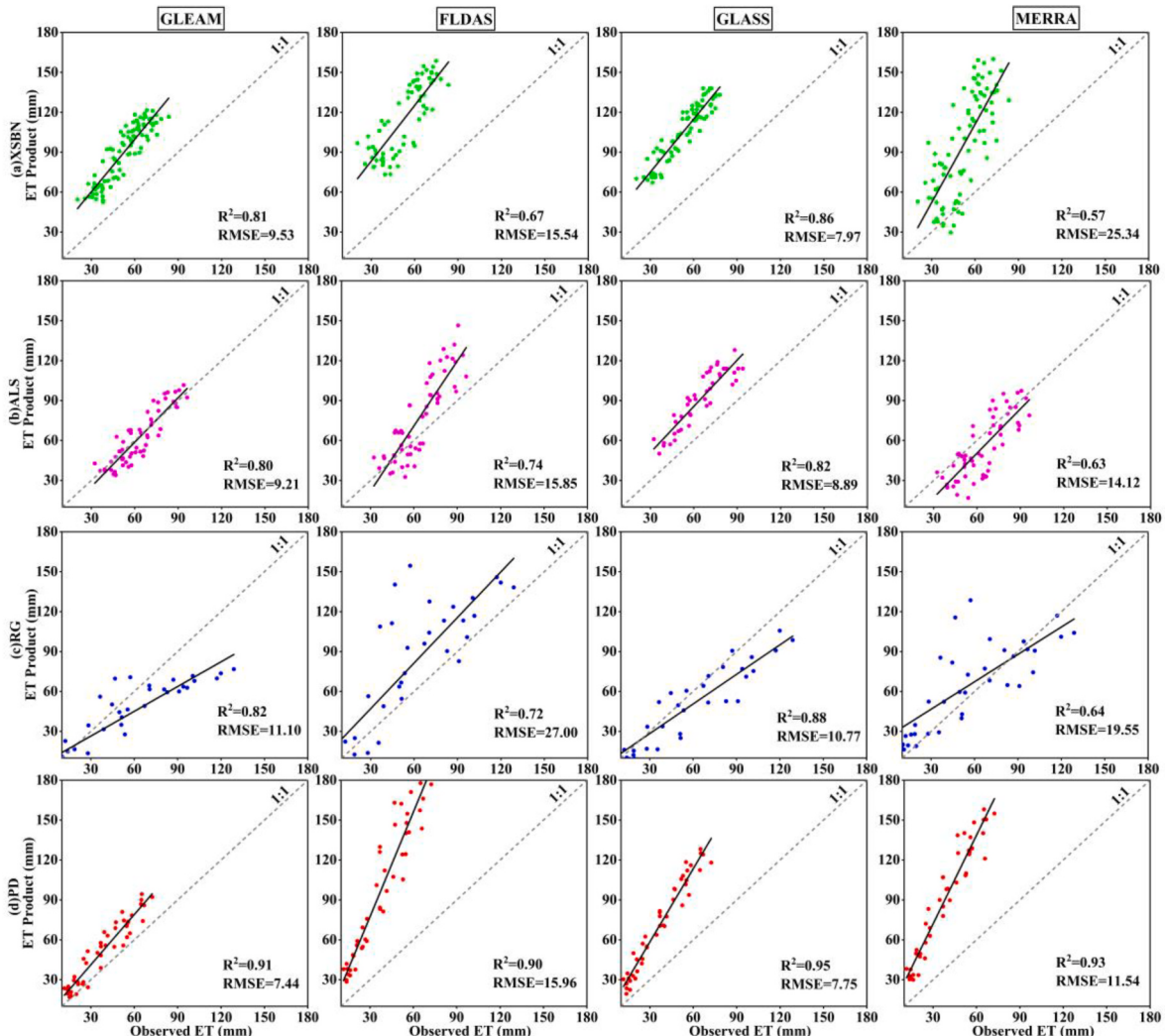


Fig. 2. The evaluations of the observed evapotranspiration (*ET*) and the four *ET* products.

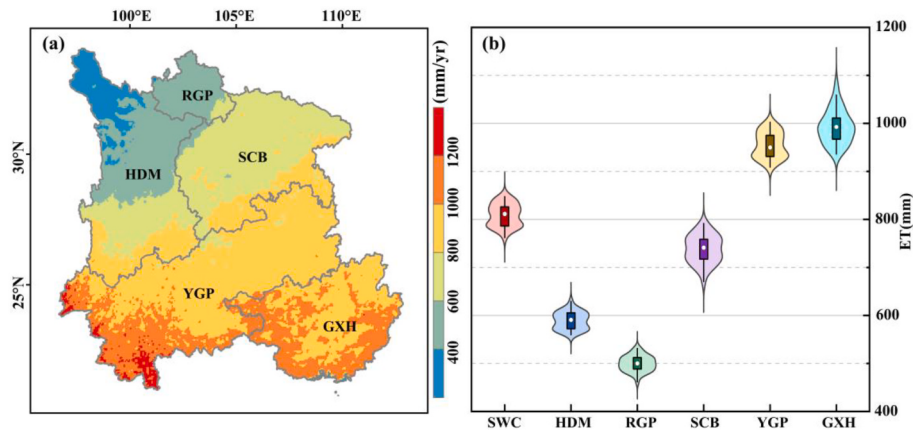


Fig. 3. The spatial distribution of multi-year mean *ET* in SWC from 1982 to 2018 (a) and the associated statistics in the sub-regions (b).

of the long-term average *ET* in SWC and its sub-regions from 1982 to 2018. As shown in Fig. 3a, the long-term average *ET* in SWC exhibits a north-to-south increasing trend. In the northwestern part of the Hengduan Mountains (HDM), the long-term average *ET* is below 400 mm. As the terrain slopes downward and the climate changes, the annual *ET* gradually increases within the HDM, exhibiting marked spatial variation. The long-term average *ET* in the Ruoergai Plateau (RGP) is relatively low, typically between 400 and 600 mm. This is mainly due to the dry climate and sparse vegetation in the high-altitude region, which reduce *ET*. In the Sichuan Basin (SCB), the long-term average *ET* is mainly concentrated between 600 and 800 mm, occupying the central part of the basin. This reflects the relatively humid but moderate *ET* characteristics of the region. The southern edges of the Guangxi Hills (GXH) and the Yunnan-Guizhou Plateau (YPG) exhibit the highest *ET*, with long-term average *ET* values exceeding 1000 mm, and some areas even reaching above 1200 mm. These regions are influenced by the tropical and subtropical monsoon climate, which delivers abundant rainfall through warm, moist airflows from the southwest and southeast. The favorable water-heat conditions and good vegetation cover contribute to the high *ET*. Fig. 3b further illustrates the statistical distribution of long-term average *ET* in SWC and its various geomorphological regions. The overall long-term average *ET* in SWC is approximately 809 mm, with a compact distribution and minimal fluctuation, indicating relatively stable *ET*. The long-term average *ET* in HDM, RGP, and SCB is 589 mm, 500 mm, and 738 mm, respectively, all of which are lower than the overall average *ET* of SWC. Among these, RGP has the lowest long-term average *ET*, with a relatively narrow distribution range. The long-term average *ET* in YGP is 955 mm, which is

mainly concentrated in the lower range. GXH has the highest long-term average *ET*, approaching 1000 mm, and its distribution range is the widest.

The spatial distribution of long-term *ET* trend changes from 1982 to 2018 (Fig. 4a) shows that the annual *ET* change rate in SWC ranges from -1 to 5 mm/yr, with most areas exhibiting a significant increasing trend ($p < 0.05$). This increase is mainly concentrated in SCB, YGP, and GXH, and the southern part of HDM. These regions are located in the upper and middle Yangtze River protective forest areas and karst ecological engineering zones, where policies like the “Grain for Green” program and the implementation of stone desertification control projects have effectively restored vegetation cover and enhanced vegetation transpiration. Regions showing a decreasing trend in *ET* are mainly found in Deyang and Ya'an cities of Sichuan Province, Yuxi and Kunming cities, and Diqing Tibetan Autonomous Prefecture of Yunnan Province, as well as Nanning in Guangxi Province. These areas are predominantly mining regions, where mineral resource extraction has led to surface cover degradation and a reduction in vegetation transpiration, thus resulting in a decreasing trend in *ET*. As shown in Fig. 4b, more than 80 % of the regions in SWC and its sub-regions show a significant increase in the long-term average *ET*, with SCB, YGP, and GXH exceeding 90 %. In summary, throughout the study period, the long-term average *ET* in SWC and its sub-regions predominantly exhibited an increasing trend, with SCB, YGP, and GXH showing a significantly higher increase in *ET* compared to other geomorphological regions.

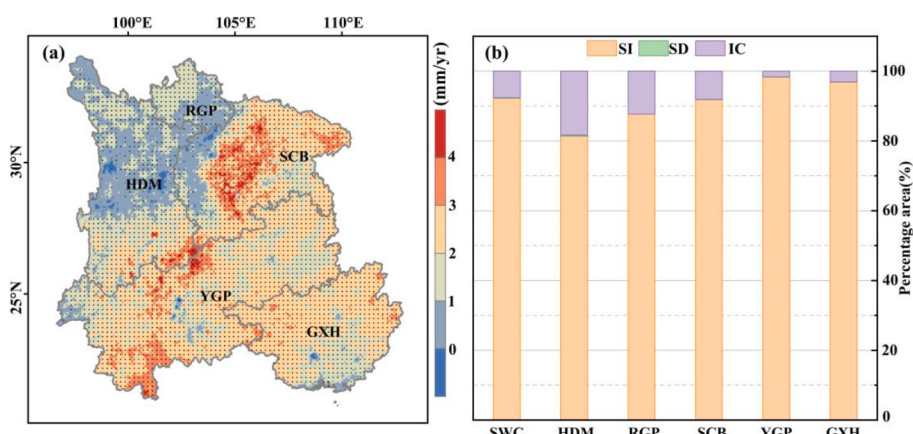


Fig. 4. The spatial trend distribution of annual *ET* from 1982 to 2018 in SWC, with the stipplings showing areas of statistical significant ($p < 0.05$) (a) and the percentage area in the sub-regions (b). SI, SD, and IC meant significant increase, significant decrease, and insignificant change, respectively.

3.3. Spatial patterns and trends of climate and vegetation

Fig. 5 shows the spatial distribution of climate factors in SWC from 1982 to 2018, including temperature (T), solar radiation (Rs), specific humidity (H), precipitation (P), wind speed (U), and leaf area index (LAI). Within the region, T , H , P , and ET exhibit similar spatial distribution characteristics, with values gradually increasing from northwest to southeast. Rs shows a clear west-high and east-low distribution pattern, with higher radiation levels in the western region, especially in the central of HDM, where Rs exceeds 212 W/m^2 . In the northeastern of SCB and YGP, Rs is relatively low, below 128 W/m^2 . The distribution of U is highly uneven, with higher wind speeds in the central of HDM and YGP, exceeding 2.8 m/s , while most areas have lower wind speeds, below 1.9 m/s . LAI is lower in the north of HDM and the middle of SCB, with values below 2, and higher in the southwest of YGP, exceeding 5.

The trend distribution of annual average T , Rs , H , P , U , and LAI from 1982 to 2018 is shown in **Fig. 6**. The trend of annual average T varies spatially, with a range of -0.02 to $0.14 \text{ }^\circ\text{C/yr}$, and 72.52% of the area shows a significant increase in T . The trend in Rs also varies spatially, with a range of -0.4 to 0.4 , and significant increases or decreases account for 14.69% and 15.75% , respectively. The trend of H ranges from -0.06 to 0.1 g/kg/yr , with 40.75% of the area showing a significant increase. The trend of annual P ranges from -9 to 15 mm/yr , with significant changes being rare, and only 5.8% of the area shows a significant increase. The trend of U ranges from -0.03 to 0.05 m/s/yr , with 43.65% of the area showing a significant increase and 21.6% showing a significant decrease. The trend of LAI ranges from -0.08 to 0.08 , with 42.54% of the area showing a significant increase. All variables exhibit an increasing trend (**Table 3**).

3.4. Attributions of long-term ET changes

Before examining the spatiotemporal patterns of driving factor contributions, we first evaluated and compared the performance of two regression approaches—OLS and ridge regression—in estimating ET responses to multiple driving variables. This comparison helps validate the robustness of the attribution results. **Table 4** summarizes the R^2 and RMSE values of both methods across five typical geomorphological regions. Ridge regression consistently outperformed OLS, with higher R^2 and lower RMSE values in all regions. This improvement indicates better handling of multicollinearity and more stable model estimates, justifying the use of ridge regression in the subsequent attribution analysis.

Fig. 7 illustrates the spatial distribution of the relative contributions of various driving factors to ET changes over the two periods, as well as the variations across subregions. This division is supported by both climatic and ecological evidence. Several studies have identified climate pattern transitions in China around the year 2000, including shifts in temperature and precipitation trends, as well as increased occurrences of abrupt drought-flood alternations (Fu et al., 2009; Zhang et al., 2023a). Concurrently, this period marks the large-scale implementation of national ecological restoration programs such as the Grain to Green Program and karst rocky desertification control projects, particularly in SWC (Lv et al., 2023; Wang et al., 2015). Thus, this temporal division enables a comparative analysis of ET dynamics under different climate regimes and land management contexts.

Across SWC, T and H consistently emerged as the dominant climatic drivers, with relative contributions exceeding 20% in both periods. Rs , U , and LAI also played important but secondary roles, each contributing over 10% , while P had the lowest impact throughout. Notably, from the first to the second period, the influence of T and H declined slightly, whereas the contributions of U and LAI increased. The relative contributions of Rs and P remained largely unchanged. These findings indicate

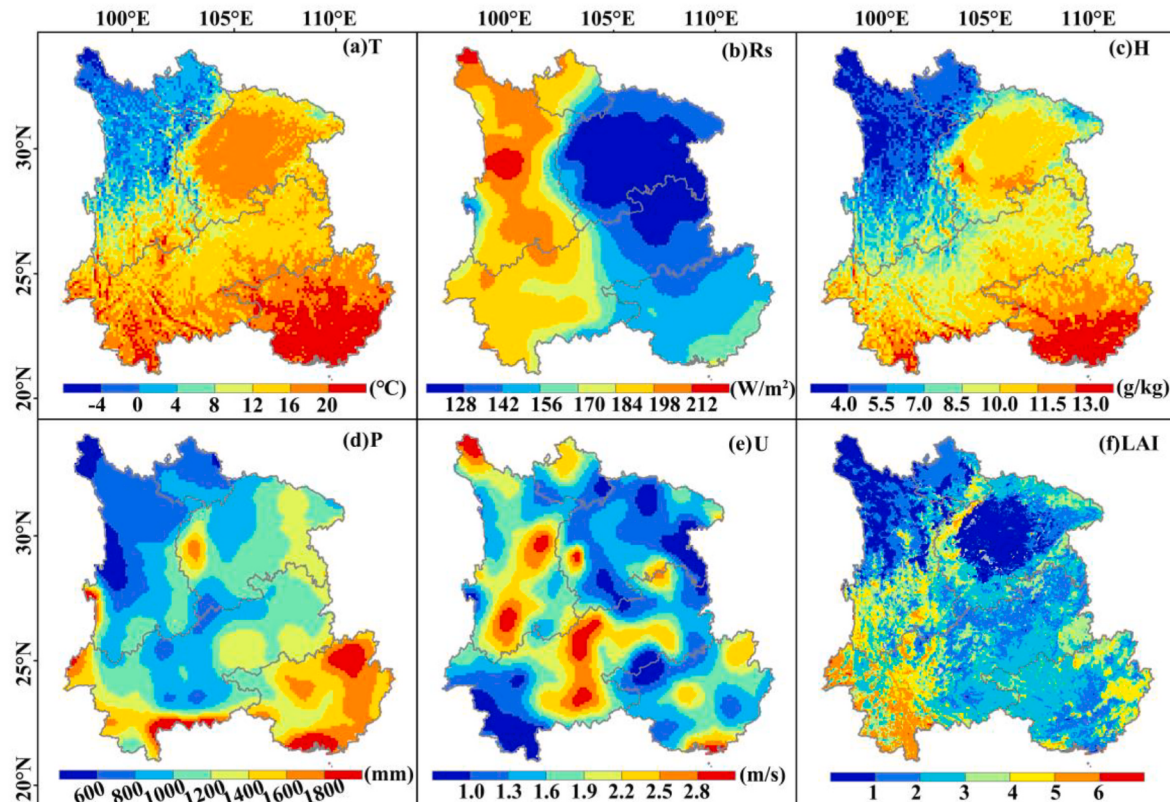


Fig. 5. The spatial distribution of the climate factors including temperature (T), solar radiation (Rs), specific humidity (H), precipitation (P), and wind speed (U) and the vegetation factor (LAI) from 1982 to 2018.

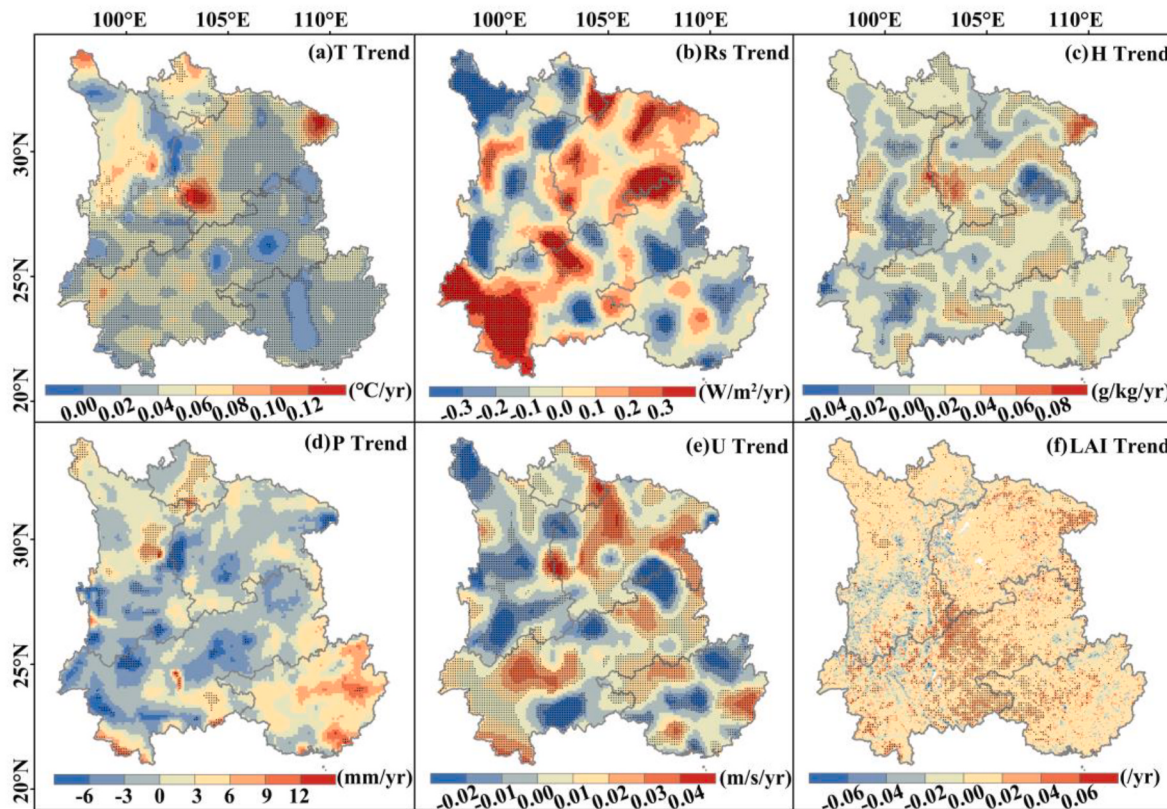


Fig. 6. The spatial trend distribution of the climate factors including T , Rs , H , P and U and the vegetation (LAI) factor from 1982 to 2018 with the stipplings showing areas of statistical significant ($p < 0.05$).

Table 3
Statistics of trends in climate variables and LAI as well as their areal percentage of significant/insignificant change.

Variables	Trend	Area Percentage(%)		
		Significant Increase	Significant Decrease	Insignificant change
Temperature ($^{\circ}\text{C}/\text{yr}$)	0.04	72.52	7.46	20.02
Downward Short Radiation ($\text{W}/\text{m}^2/\text{yr}$)	0.009	14.69	15.75	69.56
Specific Humidity ($\text{g}/\text{kg}/\text{yr}$)	0.007	40.75	17	42.25
Precipitation (mm/yr)	0.345	5.8	4.15	90.05
Wind Speed ($\text{m}/\text{s}/\text{yr}$)	0.004	43.65	21.6	34.75
LAI (/yr)	0.006	42.54	7.21	50.25

Table 4
Comparison of OLS and ridge regression models across different regions.

Region	OLS		Ridge Regression	
	R ²	RMSE	R ²	RMSE
HDM	0.75	8.21	0.83	7.45
RGP	0.68	9.02	0.76	8.10
SCB	0.71	7.80	0.86	7.25
YPG	0.70	8.70	0.78	7.90
GXH	0.75	9.50	0.88	8.70

that ET in SWC is more responsive to variations in T and H .

Across the five geomorphological regions, the dominant drivers of ET exhibited both spatial and temporal variability. In the first period, ET

changes in HDM and YGP were mainly driven by H , while T was the dominant factor in the remaining regions. In the second period, notable shifts occurred: for instance, YGP shifted from H to T as the dominant driver, while GXH exhibited the opposite trend. The contribution of U increased markedly across regions—becoming the second most influential factor in RGP, SCB, and GXH—indicating enhanced atmospheric moisture transport. From the first to the second period, T generally declined in influence across all regions, while LAI and U consistently increased, suggesting rising importance of vegetation and wind-related processes. These changes reflect region-specific interactions among climatic and ecological processes over time.

3.5. Quantification of climate and vegetation impacts on ET

Fig. 8 presents the latitudinal variation of elasticity coefficients for climate and vegetation factors, quantifying their influence on ET across SWC. A positive elasticity coefficient indicates that an increase in the driving factor leads to an increase in ET , whereas a negative value suggests an inhibiting effect on ET . Among all variables, T exhibits the strongest positive effect on ET , with an average elasticity of 0.246 and a notable peak near 30°N. In contrast, H shows the most pronounced negative influence (average elasticity -0.047), with substantial fluctuations across latitudes. Other factors have comparatively smaller effects: Rs and LAI have weak but generally positive influences, while U shows modest positive contributions with regional peaks. P displays near-zero average elasticity, indicating minimal and inconsistent influence. Overall, ET is most sensitive to temperature increases and humidity reductions, with latitude-dependent variability reflecting the region's complex climatic gradients.

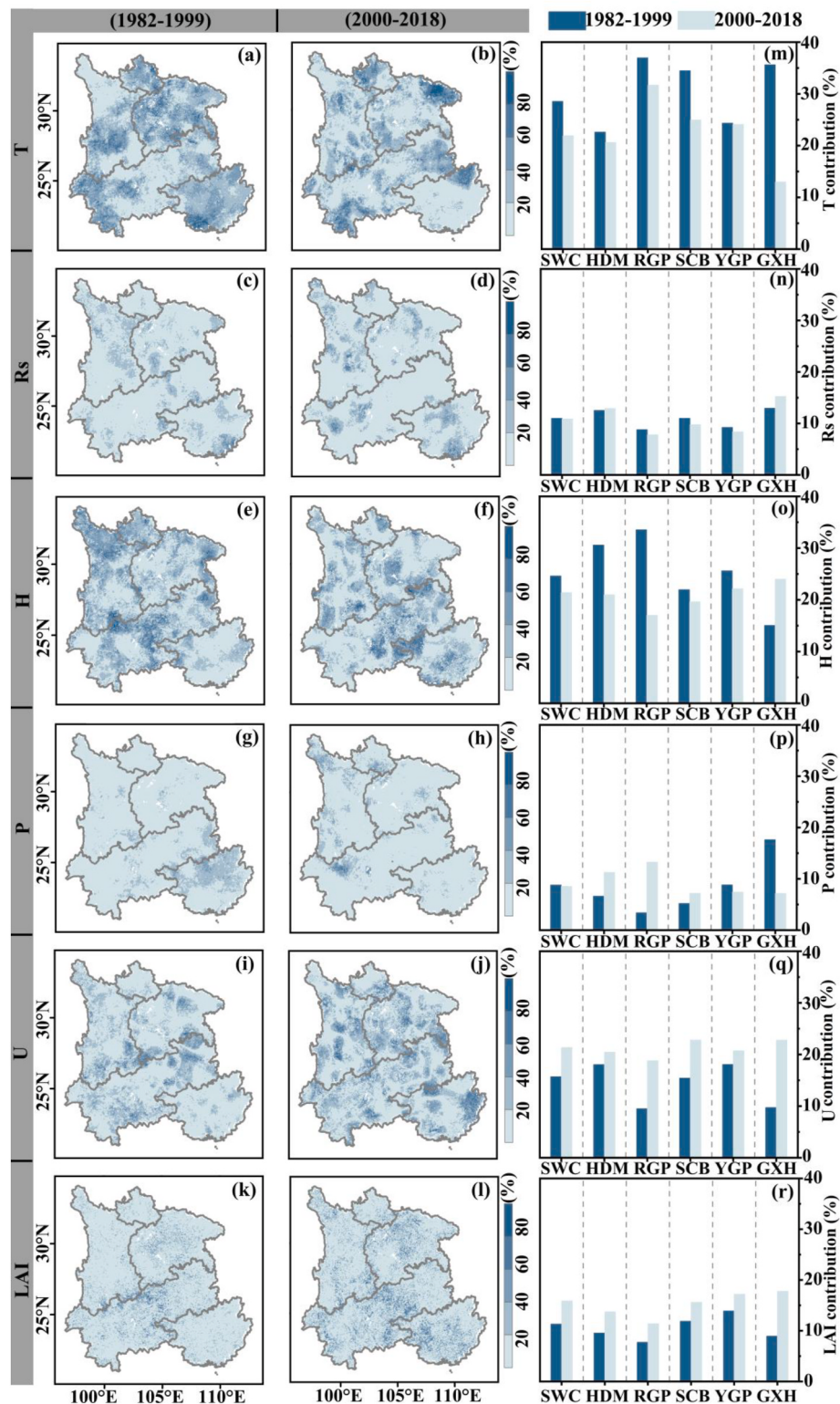


Fig. 7. The relative contributions of the climate factors including T , Rs , H , P and U and the vegetation factor (LAI) in two stages (al). The bar chart showed the relative contributions in the sub-regions (m ~ r).

4. Discussion

4.1. Spatiotemporal variations in ET

ET plays a critical role in regulating regional water and energy balances, particularly in ecologically fragile and climatically diverse

regions such as SWC. In recent years, with the increasing influence of climate change and human activities, as well as changes in vegetation structure and environmental factors, pronounced alterations have occurred in both regional and global ET processes (Allen and Ingram, 2002; Madakumbura et al., 2019). Many studies have reported a significant decline in pan evaporation over recent decades despite ongoing

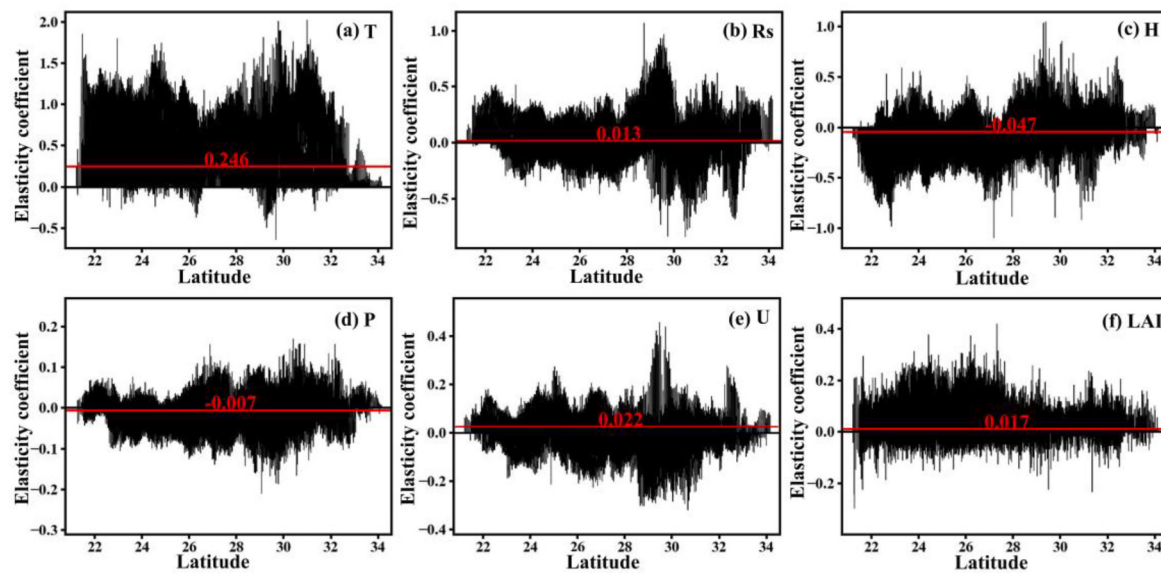


Fig. 8. The latitudinal distribution of the elasticity coefficients for ET driving factors in SWC. The mean values were denoted in red.

climate warming (Liu et al., 2011; Roderick and Farquhar, 2002). This phenomenon, termed the “evaporation paradox,” reflects a contradiction between the expected increase in evaporative demand and the observed decrease in measured evaporation. Additionally, remote sensing and model-based studies consistently show increasing global ET trends since the 1980s (Jung et al., 2010; Pan et al., 2020; Wang et al., 2021b, 2022a; Zhang et al., 2016a).

In this study, ET in SWC exhibited an increasing trend of 1.92 mm/yr from 1982 to 2018, and ET in all geomorphological subregions also exhibited an increasing trend. This finding aligns with the conclusions of Li et al. (2021) and Zheng et al. (2022), who observed strong ET growth in SWC, particularly in the karst regions. Spatially, ET increased from north to south, with the highest values in the Guangxi Hills (GXH), followed by the Yunnan-Guizhou Plateau (YGP), and the lowest in the Ruoergai Plateau (RGP). This spatial pattern is consistent with previous research (Cheng et al., 2021). The subtropical monsoon climate in GXH, combined with diverse vegetation and abundant precipitation, supports high transpiration and evaporation. In contrast, the high elevation and cooler temperatures of RGP limit ET potential despite moderate precipitation.

4.2. Climate drivers of ET change

Our results indicate that T and H are the dominant climate drives of ET variability in SWC, each contributing over 20 % in both study phases. This conclusion aligns with those of Fu et al. (2022) and Zheng et al. (2022), who identified T and H as the primary drivers of ET change in SWC. The strong influence of T reflects its role in supplying energy for evapotranspiration. H contributes by regulating vapor pressure gradients, which in turn affect atmospheric moisture flux. The stable but smaller contributions of Rs and U suggest that they function as supplementary energy sources and enhance convective transport. P showed the weakest contribution, consistent with previous studies that have shown ET 's response to P is weaker in humid climates compared to arid ones (Liu et al., 2016; Zhang et al., 2019). SWC, characterized by a humid climate, abundant water resources, and relatively high soil moisture content, experiences ET primarily driven by energy factors (such as T and Rs) and diffusion factors (such as H and U) in this moisture-sufficient environment.

The dominant factors of ET vary significantly across different geomorphological regions and exhibit stage-dependent evolutionary characteristics. Studies have shown that the 1980s were the period when

the global land surface temperature increased at the fastest rate (Foster and Rahmstorf, 2011; Lawrimore et al., 2011; Sun et al., 2017; Wang et al., 2017). Thus, the first stage marks a substantial period of global warming, where the rise in T provided strong energy driving for ET . However, in the second stage, the global warming slowed down, reducing the driving effect of T on ET . The overall high cloud cover in SWC limits the variation in Rs , leading to a relatively stable contribution of Rs to ET in both stages. This indicates that Rs , as an energy-driving factor, maintains a resilient fundamental role in humid climate regions (Penman, 1948). The influence of H on the ET rate primarily lies in regulating the water vapor pressure difference in the air. In GXH, where P is abundant, especially during the second stage with sustained rainfall, the specific humidity of the air increased. As P increased, soil moisture became sufficient, humidity rose, and the water vapor pressure difference decreased, making H 's relative contribution to ET more notable. HDM and RGP, situated in the transition zone between arid and humid climates, experienced a direct impact on soil moisture and plant growth due to the increase in P during the second stage. This led to a evident rise in the relative contribution of P to ET in these regions. Although China as a whole has experienced a “surface stabilization” phenomenon, in certain areas, especially in SWC, U showed an increasing trend after 2000 (Liu et al., 2019; Yang et al., 2012), which directly enhanced the diffusion effect of U on ET .

4.3. Influence of vegetation factors on ET change

Vegetation transpiration is a major contributor to ET (Zhang et al., 2020), especially in humid climate regions, where plants release substantial water, directly affecting the hydrological cycle and energy exchange. Vegetation impacts transpiration rate through its structural characteristics (such as leaf area and stomatal density), physiological processes (such as photosynthesis and transpiration regulation), and ecological traits (such as root distribution), which in turn affect regional ET (Sun et al., 2020). The results indicate that LAI increases in SWC contribute over 10 % to ET changes, particularly in the second phase, where its relative contribution has risen across SWC and its subregions. SWC is rich in vegetation resources (Piao et al., 2009), but the vegetation in this region is highly vulnerable to climate change, and its self-restoration capacity is constrained by the widespread karst topography (Liu et al., 2018; Peng et al., 2011). To tackle these challenges, SWC has implemented various ecological restoration projects since 2000, including the Grain to Green Project and Resistance to Karst

Rocky Desertification (Mao et al., 2022), resulting in rapid vegetation recovery (Ma et al., 2023; Yan et al., 2021).

However, vegetation greening has significantly increased regional transpiration, thereby increasing water evaporation losses (Bai et al., 2020; Tian et al., 2017). Studies indicate that vegetation communities with high leaf area index evidently increase the demand for soil moisture and groundwater resources, exacerbating regional water resource pressure. The water supply in karst regions is already limited, and large-scale vegetation restoration may compete with agricultural, industrial, and residential water use. A healthy ecosystem and hydrological cycle are the foundation for the sustainable development of karst areas. Therefore, by optimizing vegetation restoration strategies and scientifically managing water resources, it is possible to effectively enhance the resilience of the ecosystem in karst regions, promote sustainable development, and provide strong ecological support for the regional economy and society.

Moreover, while LAI effectively reflects vegetation greenness and phenology, it does not differentiate between vegetation types, each of which has distinct eco-hydrological characteristics. To further explore this aspect, we analyzed the annual ET for six land cover types—forest, shrub, grassland, cropland, barren, and water—during the two study periods (1982–1999 and 2000–2018) (Fig. 9). The results reveal that forested areas consistently exhibit the highest ET values, averaging over 850 mm/yr, due to their dense canopy structures and deep rooting systems which facilitate higher transpiration rates. Croplands and grasslands follow with moderate ET levels, reflecting seasonal variability and agricultural water use. Shrubs maintain lower ET values, while barren lands show the lowest, typically under 500 mm/yr, reflecting their sparse vegetation and limited evapotranspiration potential. Notably, the ET differences among vegetation types have remained relatively stable across the two periods, although slight increases are observed in croplands and forests after 2000. These findings demonstrate that LAI alone cannot capture the heterogeneity in eco-hydrological functioning, and vegetation classification is essential for robust ET attribution.

4.4. Quantitative attribution analysis

This study uses a double logarithmic elasticity model to quantitatively analyze the effects of climate and vegetation changes on ET in SWC. The average elasticity coefficients of T , Rs , H , P , U , and LAI on ET are 0.246, 0.013, -0.147, -0.007, 0.022, and 0.017, respectively. This means that for every 10 % increase in T , Rs , U , and LAI, ET will increase by 2.46 %, 0.13 %, 0.22 %, and 0.17 %, respectively. In contrast, a 10 % increase in H and P will lead to a decrease in ET by 1.47 % and 0.07 %, respectively. The study finds that T has the highest positive elasticity coefficient for ET, whereas H exhibits the strongest negative elasticity coefficient. This conclusion quantitatively confirms that T and H are the dominant factors driving ET changes in SWC. The negative elasticity

coefficients of H and P suggest that both factors negatively influence ET variations in the region.

ET is mainly driven by the vapor pressure gradient between the air and plant leaves or soil surface. As H increases, the vapor pressure difference decreases, which leads to a reduction in ET rates. Furthermore, under high humidity conditions, plants close their stomata to reduce water loss, further lowering the transpiration rate. The negative elasticity coefficient for P is mainly due to the fact that, in high-altitude areas such as RGP and HDM, the region is limited by heat and radiation, causing an increase in P to primarily result in runoff or underground seepage (Duan and Duan, 2020). Additionally, the negative impact of P is seen in the mismatch between P and ET demand in SWC. During the rainy season, P is abundant, but Rs and T are relatively low, resulting in lower ET demand. In contrast, during the dry season, although ET demand is high, P is insufficient, leading to a seasonal mismatch that negatively affects ET.

4.5. Uncertainty analysis and future perspectives

4.5.1. Sources and propagation of uncertainty

This study employs multi-source remote sensing datasets and a regression-based modeling framework to investigate the spatiotemporal variations and driving mechanisms of ET across Southwest China from 1982 to 2018. Nevertheless, some uncertainties remain, which may affect the spatial robustness and accuracy of the attribution results.

From a data perspective, although the CMFD meteorological dataset and GLASS LAI product employed in this study offer broad spatial and temporal coverage, estimation errors may still occur in regions with complex terrain, sparse station distribution, or limited remote sensing observability. These data uncertainties may propagate through the model, influencing the robustness of regression coefficients and the consistency of attribution results. In terms of model construction, ridge regression effectively mitigates multicollinearity, and the use of pixel-wise adaptive λ values enhances local modeling stability. Nevertheless, the model outcomes may remain sensitive to fluctuations in input variables, especially in areas where boundary values change frequently, potentially resulting in unstable attribution structures. Furthermore, the elasticity model assumes a log-linear relationship between variables, which does not capture potential interaction effects, nonlinear responses, or lagged feedbacks. This structural simplification limits the model's ability to characterize complex eco-hydrological processes.

Future studies may consider incorporating nonlinear regression methods, structural equation modeling, and uncertainty propagation frameworks to better identify and quantify sources of uncertainty within the model, thereby improving the reliability and explanatory power of the attribution analysis.

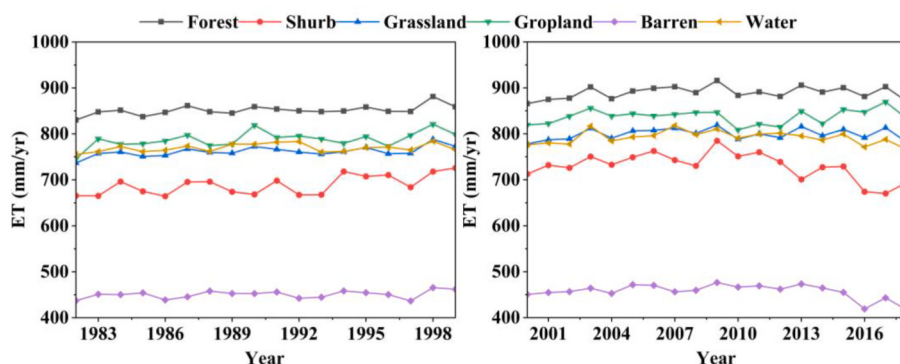


Fig. 9. Annual mean ET for different land cover types in SWC from 1982 to 2018.

4.5.2. Future perspectives: toward an integrated “diagnosis–prediction” framework

To enhance the capacity of *ET* studies to transition from historical attribution to future projection, we propose the development of an integrated “diagnosis–prediction” modeling framework. On one hand, the ridge regression and elasticity-based analytical system developed in this study can be used to identify the dominant driving factors of *ET* changes under different climatic and ecological conditions. On the other hand, combining regional climate models, CMIP6 multi-scenario data, and LUH2 land-use trajectories can support scenario-based *ET* simulations, contributing to long-term water resource management and ecological planning.

This integrated framework offers the potential to unify historical diagnostics and future simulations, advancing *ET* modeling from static interpretation to dynamic forecasting, and providing forward-looking support for hydrological modeling in ecologically fragile regions.

5. Conclusions

This study integrates remote sensing and meteorological data with ridge regression and double-log elasticity models to analyze *ET* dynamics and driving factors in SWC from 1982 to 2018. The results indicate that *ET* in SWC follows a spatial pattern increasing from south to north, with annual average values ranging from 500 mm on the high-altitude Ruoergai Plateau to 1000 mm in the Guangxi Hills. Most regions in the study area exhibit a significant increasing trend, particularly where vegetation restoration and ecological engineering projects have been implemented.

Temperature and specific humidity are the primary climate factors driving *ET* changes, each contributing over 20 % in both phases. Temperature has the highest positive elasticity coefficient (0.246), indicating its strongest enhancement effect on *ET*, while specific humidity has the largest negative elasticity coefficient (-0.147), reflecting its most marked suppressive effect. The relative contribution of vegetation factors (*LAI*) has significantly increased, especially in the second phase following the implementation of ecological projects. The dominant

factors influencing *ET* changes vary by geomorphological region and phase. In the Hengduan Mountains and the Yunnan-Guizhou Plateau, *ET* was primarily driven by specific humidity in the first phase, whereas temperature emerged as the dominant factor in the second phase. In the Guangxi Hills, wind speed and specific humidity have evidently higher relative contributions in the second phase.

The combined effects of climate change and vegetation restoration have significantly contributed to the observed increase in *ET* across Southwest China. While greening enhances ecosystem resilience and climate adaptation, it may also aggravate regional water stress—particularly in hydrologically vulnerable areas such as the karst landscapes of the Yunnan-Guizhou Plateau. Therefore, restoration strategies must be aligned with local water resource carrying capacities to avoid unintended ecological risks. Region-specific approaches are essential: in the Hengduan Mountains, priority should be given to slope stabilization and forest protection; in the Ruoergai Plateau, grazing regulation and alpine wetland preservation are key; in the Sichuan Basin, coordinated urban-agricultural water allocation is needed; in the Yunnan-Guizhou Plateau, strict vegetation-water balance thresholds should be monitored; and in the Guangxi Hills, the management of forest density and moisture recycling is crucial. These differentiated recommendations aim to reconcile ecological restoration with water security and are summarized in Appendix Table A1. Overall, balancing vegetation expansion with hydrological limits is fundamental to enhancing the long-term effectiveness and sustainability of restoration efforts.

CRediT authorship contribution statement

Yanjun Wang: Writing – original draft, Data curation. **Xiaorong Huang:** Funding acquisition. **Yi Ao:** Validation.

Declaration of competing interest

The authors declare that they have no known competing financial interests or personal relationships that could have appeared to influence the work reported in this paper.

Appendix

Table A1

Recommended water-ecosystem management strategies in the sub-regions.

Region	Management Focus	Recommended Measures
HDM	Forest restoration and slope stabilization	Strengthen natural forest conservation, restrict overexploitation, and maintain forest cover in high-altitude areas to reduce runoff variability.
RGP	Wetland conservation and grazing control	Prevent wetland degradation and grassland deterioration through rotational grazing and grazing bans to enhance water retention capacity.
SCB	Urban-agricultural water coordination and agricultural water-saving	Promote irrigation system reforms, improve water use efficiency, and prevent excessive agricultural abstraction from affecting downstream flows.
YPG	Regulation of greening intensity in karst regions	Avoid large-scale planting of high water-consuming species; set vegetation cover thresholds based on local water resource carrying capacity to prevent groundwater overdraft.
GXH	Forest density management and moisture recycling enhancement	Adjust plantation density, preserve understory vegetation, and promote stability of regional atmospheric moisture recycling.

Data availability

I have shared the link from where the data can be accessed free off charge.

References

- Ahiablame, L., Sheshukov, A.Y., Rahmani, V., Moriasi, D., 2017. Annual baseflow variations as influenced by climate variability and agricultural land use change in the Missouri River Basin. *J. Hydrol.* 551, 188–202. <https://doi.org/10.1016/j.jhydrol.2017.05.055>.
- Allen, M.R., Ingram, W.J., 2002. Constraints on future changes in climate and the hydrologic cycle. *Nature* 419 (6903). <https://doi.org/10.1038/nature01092>, 224–.

- Bai, P., Liu, X.M., Zhang, Y.Q., Liu, C.M., 2020. Assessing the impacts of vegetation greenness change on evapotranspiration and water yield in China. *Water Resour. Res.* 56 (10). <https://doi.org/10.1029/2019wr027019>.
- Cai, W.J., Jiang, X.H., Sun, H.T., He, J.Y., Deng, C., Lei, Y.X., 2022. Temporal and spatial variation and driving factors of water consumption in the middle Heihe river basin before and after the implementation of the "97 water diversion scheme". *Agric. Water Manag.* 269. <https://doi.org/10.1016/j.agwat.2022.107727>.
- Chen, P., Wang, S., Song, S., Wang, Y., Wang, Y., Gao, D., Li, Z., 2022. Ecological restoration intensifies evapotranspiration in the Kubuqi Desert. *Ecol. Eng.* 175. <https://doi.org/10.1016/j.ecoleng.2021.106504>.
- Chen, W., Wang, S., Niu, S., 2023. A dataset of carbon, water and heat fluxes of Zoige alpine meadow from 2015 to 2020. *Chinese Scientific Data* 8 (2). <https://doi.org/10.11922/11-6035.csd.2023.0009.zh>.
- Cheng, M., Jiao, X., Jin, X., Li, B., Liu, K., Shi, L., 2021. Satellite time series data reveal interannual and seasonal spatiotemporal evapotranspiration patterns in China in response to effect factors. *Agric. Water Manag.* 255. <https://doi.org/10.1016/j.agwat.2021.107046>.
- Duan, Q., Duan, A., 2020. The energy and water cycles under climate change. *Natl. Sci. Rev.* 7 (3), 553–557. <https://doi.org/10.1093/nsr/nwaa003>.
- Fang, B.J., Lei, H.M., Zhang, Y.C., Quan, Q., Yang, D.W., 2020. Spatio-temporal patterns of evapotranspiration based on upscaling eddy covariance measurements in the dryland of the North China Plain. *Agric. For. Meteorol.* 281. <https://doi.org/10.1016/j.agrformet.2019.107844>.
- Fisher, J.B., Melton, F., Middleton, E., Hain, C., Anderson, M., Allen, R., McCabe, M.F., Hook, S., Baldocchi, D., Townsend, P.A., Kilic, A., Tu, K., Miralles, D.D., Perret, J., Lagouarde, J.P., Waliser, D., Purdy, A.J., French, A., Schimel, D., Famiglietti, J.S., Stephens, G., Wood, E.F., 2017. The future of evapotranspiration: global requirements for ecosystem functioning, carbon and climate feedbacks, agricultural management, and water resources. *Water Resour. Res.* 53 (4), 2618–2626. <https://doi.org/10.1002/2016wr020175>.
- Foster, G., Rahmstorf, S., 2011. Global temperature evolution 1979–2010. *Environ. Res. Lett.* 6 (4). <https://doi.org/10.1088/1748-9326/6/4/044022>.
- Fu, G.B., Charles, S.P., Yu, J.J., Liu, C.M., 2009. Decadal climatic variability, trends, and future scenarios for the North China Plain. *J. Clim.* 22 (8), 2111–2123. <https://doi.org/10.1175/2008jcli2605.1>.
- Fu, J., Gong, Y., Zheng, W., Zou, J., Zhang, M., Zhang, Z., Qin, J., Liu, J., Quan, B., 2022. Spatial-temporal variations of terrestrial evapotranspiration across China from 2000 to 2019. *Sci. Total Environ.* 825. <https://doi.org/10.1016/j.scitotenv.2022.153951>.
- Fu, J.Y., Wang, W.G., Liu, B.J., Lu, Y., Xing, W.Q., Cao, M.Z., Zhu, S.F., Guan, T.S., Wei, J., Chen, Z.F., 2023. Seasonal divergence of evapotranspiration sensitivity to vegetation changes—A proportionality-hypothesis-based analytical solution. *J. Hydrol.* 617. <https://doi.org/10.1016/j.jhydrol.2022.129055>.
- Geng, J.W., Li, H.P., Pang, J.P., Zhang, W.S., Shi, Y.J., 2022. The effects of land-use conversion on evapotranspiration and water balance of subtropical forest and managed tea plantation in Taihu Lake Basin, China. *Hydrolog. Process.* 36 (8). <https://doi.org/10.1002/hyp.14652>.
- Hao, L., Pan, C., Fang, D., Zhang, X.Y., Zhou, D.C., Liu, P.L., Liu, Y.Q., Sun, G., 2018. Quantifying the effects of overgrazing on mountainous watershed vegetation dynamics under a changing climate. *Sci. Total Environ.* 639, 1408–1420. <https://doi.org/10.1016/j.scitotenv.2018.05.224>.
- Jongen, H.J., Vulova, S., Meier, F., Steeneveld, G.J., Jansen, F.A., Tetzlaff, D., Kleinschmit, B., Haacke, N., Teuling, A.J., 2024. Attributing urban evapotranspiration from eddy-covariance to surface cover: bottom-up versus top-down. *Water Resour. Res.* 60 (9). <https://doi.org/10.1029/2024wr037508>.
- Jung, M., Reichstein, M., Ciais, P., Seneviratne, S.I., Sheffield, J., Goulden, M.L., Bonan, G., Cescatti, A., Chen, J., de Jeu, R., Dolman, A.J., Eugster, W., Gerten, D., Gianelle, D., Gobron, N., Heinke, J., Kimball, J., Law, B.E., Montagnani, L., Mu, Q., Mueller, B., Oleson, K., Papale, D., Richardson, A.D., Roupsard, O., Running, S., Tomelleri, E., Viovy, N., Weber, U., Williams, C., Wood, E., Zaehle, S., Zhang, K., 2010. Recent decline in the global land evapotranspiration trend due to limited moisture supply. *Nature* 467 (7318), 951–954. <https://doi.org/10.1038/nature09396>.
- Kendall, M.G., 1990. Rank correlation methods. *Br. J. Psychol.* 25 (1), 86–91. <https://doi.org/10.2307/2333282>.
- Lawrimore, J.H., Menne, M.J., Gleason, B.E., Williams, C.N., Wuertz, D.B., Vose, R.S., Rennie, J., 2011. An overview of the Global Historical Climatology Network monthly mean temperature data set, version 3. *J. Geophys. Res. Atmos.* 116. <https://doi.org/10.1029/2011jd016187>.
- Li, S.J., Wang, G.J., Sun, S.L., Hagan, D.F.T., Chen, T.X., Dolman, H., Liu, Y., 2021. Long-term changes in evapotranspiration over China and attribution to climatic drivers during 1980–2010. *J. Hydrol.* 595. <https://doi.org/10.1016/j.jhydrol.2021.126037>.
- Li, S.J., Wang, G.J., Zhu, C.X., Lu, J., Ullah, W., Hagan, D.F.T., Kattel, G., Peng, J., 2022. Attribution of global evapotranspiration trends based on the Budyko framework. *Hydrolog. Earth Syst. Sci.* 26 (13), 3691–3707. <https://doi.org/10.5194/hess-26-3691-2022>.
- Li, X.L., Xu, X.F., Sonnenborg, T.O., Andreassen, M., He, C.S., 2024. Effect of ecological restoration on evapotranspiration and water yield in the agro-pastoral ecotone in northern China during 2000–2018. *J. Hydrol.* 638. <https://doi.org/10.1016/j.jhydrol.2024.131531>.
- Liu, H., Zhang, M., Lin, Z., Xu, X., 2018. Spatial heterogeneity of the relationship between vegetation dynamics and climate change and their driving forces at multiple time scales in Southwest China. *Agric. For. Meteorol.* 256, 10–21. <https://doi.org/10.1016/j.agrformet.2018.02.015>.
- Liu, J., Jia, B., Xie, Z., Shi, C., 2016. Ensemble simulation of land evapotranspiration in China based on a multi-forcing and multi-model approach. *Adv. Atmos. Sci.* 33 (6), 673–684. <https://doi.org/10.1007/s00376-016-5213-0>.
- Liu, J.Y., You, Y.Y., Li, J.F., Sitch, S., Gu, X.H., Nabel, J., Lombardozzi, D., Luo, M., Feng, X.Y., Arneth, A., Jain, A.K., Friedlingstein, P., Tian, H.Q., Poulter, B., Kong, D., 2021. Response of global land evapotranspiration to climate change, elevated CO₂, and land use change. *Agric. For. Meteorol.* 311, 14. <https://doi.org/10.1016/j.agrformet.2021.108663>.
- Liu, X.M., Luo, Y.Z., Zhang, D., Zhang, M.H., Liu, C.M., 2011. Recent changes in pan-evaporation dynamics in China. *Geophys. Res. Lett.* 38. <https://doi.org/10.1029/2011gl047929>.
- Liu, Z., Dong, Z., Zhang, Z., Cui, X., Xiao, N., 2019. Spatial and temporal variation of the near-surface wind regimes in the Taklimakan Desert, Northwest China. *Theor. Appl. Climatol.* 138 (1–2), 433–447. <https://doi.org/10.1007/s00704-019-02824-w>.
- Lu, X.X., Sheng, M.Y., Luo, M.X., 2024. Knowledge mapping analysis of Karst Rocky desertification vegetation restoration in Southwest China: study based on web of science literature. *Agronomy* 14 (10). <https://doi.org/10.3390/agronomy14102235>.
- Lv, Y., Zhang, L., Li, P., He, H.L., Ren, X.L., Zhang, M.Y., 2023. Ecological restoration projects enhanced terrestrial carbon sequestration in the karst region of Southwest China. *Front. Ecol. Evolut.* 11. <https://doi.org/10.3389/fevo.2023.1179608>.
- Ma, B., He, C., Jing, J., Wang, Y., Bing, L., He, H., 2023. Attribution of vegetation dynamics in Southwest China from 1982 to 2019. *Acta Geogr. Sin.* 78 (3), 714–728. <https://doi.org/10.1182/dlxb202303013>.
- Madakumbura, G.D., Kim, H., Utsumi, N., Shiogama, H., Fischer, E.M., Seland, O., Scinocca, J.F., Mitchell, D.M., Hirabayashi, Y., Oki, T., 2019. Event-to-event intensification of the hydrologic cycle from 1.5 °C to a 2 °C warmer world. *Sci. Rep.* 9. <https://doi.org/10.1038/s41598-019-39936-2>.
- Mann, H.B., 1945. Nonparametric tests against trend. *Econometrica* 13 (3), 245–259. <https://doi.org/10.2307/1907187>.
- Mao, Y., Jiang, Y., Zhang, C., Qiao, Y., Lv, T., Qiu, J., 2022. Spatio-temporal changes and influencing factors of vegetation net primary productivity in southwest China in the past 20 years and its response to ecological engineering. *Acta Ecol. Sin.* 42 (7), 2878–2890. <https://doi.org/10.5846/stxb202101260270>.
- McNally, A., 2018. FLDAS Noah Land Surface Model L4 Global Monthly 0.1 x 0.1 degree (MERRA-2 and CHIRPS), Greenbelt, MD, USA, Goddard Earth Sciences Data and Information Services Center (GES DISC). <https://doi.org/10.5067/5NHNC2T9375G>.
- Miralles, D.G., Holmes, T.R.H., De Jeu, R.A.M., Gash, J.H., Meesters, A., Dolman, A.J., 2011. Global land-surface evaporation estimated from satellite-based observations. *Hydrolog. Earth Syst. Sci.* 15 (2), 453–469. <https://doi.org/10.5194/hess-15-453-2011>.
- Pan, S., Pan, N., Tian, H., Friedlingstein, P., Sitch, S., Shi, H., Arora, V.K., Haverd, V., Jain, A.K., Kato, E., Lienert, S., Lombardozzi, D., Nabel, J.E.M.S., Otte, C., Poulter, B., Zaehle, S., Running, S.W., 2020. Evaluation of global terrestrial evapotranspiration using state-of-the-art approaches in remote sensing, machine learning and land surface modeling. *Hydrolog. Earth Syst. Sci.* 24 (3), 1485–1509. <https://doi.org/10.5194/hess-24-1485-2020>.
- Pei, T.T., Wu, X.C., Li, X.Y., Zhang, Y., Shi, F.Z., Ma, Y.J., Wang, P., Zhang, C.C., 2017. Seasonal divergence in the sensitivity of evapotranspiration to climate and vegetation growth in the Yellow River Basin, China. *J. Geophys. Res.-Biogeosci* 122 (1), 103–118. <https://doi.org/10.1002/2016jg003648>.
- Peng, J., Xu, Y., Cai, Y., Xiao, H., 2011. Climatic and anthropogenic drivers of land use/cover change in fragile karst areas of southwest China since the early 1970s: a case study on the Maotiaohuo watershed. *Environ. Earth Sci.* 64 (8), 2107–2118. <https://doi.org/10.1007/s12665-011-1037-5>.
- Penman, H.L., 1948. Natural evaporation from open water, bare soil and grass. *Proc. Roy. Soc. of London, Ser. A.* 193 (1032), 120–145. <https://doi.org/10.2307/98151>.
- Pereira, L.S., Allen, R.G., Smith, M., Raes, D., 2015. Crop evapotranspiration estimation with FAO56: past and future. *Agric. Water Manag.* 147, 4–20. <https://doi.org/10.1016/j.agwat.2014.07.031>.
- Piao, S., Fang, J., Ciais, P., Peylin, P., Huang, Y., Sitch, S., Wang, T., 2009. The carbon balance of terrestrial ecosystems in China. *Nature* 458 (7241). <https://doi.org/10.1038/nature07944>, 1009–U82.
- Qi, D., Fei, X., Song, Q., Zhang, Y., Sha, L., Liu, Y., Zhou, W., Lu, Z., FanZexin, 2021a. A dataset of carbon and water fluxes observation in subtropical evergreen broad-leaved forest in Ailao Shan from 2009 to 2013. *China Scient. Data* 6 (1). <https://doi.org/10.11922/csdata.2020.0089.zh>.
- Qi, D., Zhang, Y., Song, Q., Fei, X., Sha, L., Liu, Y., Zhou, W., Zhou, L., Deng, X., Luo, Y., Deng, Y., 2021b. A dataset of carbon, water and energy fluxes observed in Xishuangbanna tropical seasonal rain forest from 2003 to 2010. *China Scient. Data* 6 (1). <https://doi.org/10.11922/csdata.2020.0037.zh>.
- Reichle, R.H., Koster, R.D., De Lannoy, G.J.M., Forman, B.A., Liu, Q., Mahanama, S.P.P., Touré, A., 2011. Assessment and enhancement of MERRA land surface hydrology estimates. *J. Clim.* 24 (24), 6322–6338. <https://doi.org/10.1175/jcli-d-10-05033.1>.
- Ren, H.Y., Tan, K., Zhang, G.Y., Wang, Z.P., Shi, H.J., Wen, Z.M., Liu, Y.Y., 2024. Diverse responses of the changes in evapotranspiration and water yield to vegetation and climate change in the Yanhe River watershed. *Ecol. Indic.* 168. <https://doi.org/10.1016/j.ecolind.2024.112750>.
- Roderick, M.L., Farquhar, G.D., 2002. The cause of decreased pan evaporation over the past 50 years. *Science* 298, 1410–1411. <https://doi.org/10.1126/science.1075390-a>.
- Sankarasubramanian, A., Vogel, R.M., Limbrunner, J.F., 2001. Climate elasticity of streamflow in the United States. *Water Resour. Res.* 37 (6), 1771–1781. <https://doi.org/10.1029/2000wr900330>.
- Sen, P.K., 1968. Estimates of the regression coefficient based on Kendall's tau. *J. Am. Stat. Assoc.* 63 (324), 1379–1389. <https://doi.org/10.1080/01621459.1968.10480934>.
- Shan, N., Shi, Z., Yang, X., Gao, J., Cai, D., 2015. Spatiotemporal trends of reference evapotranspiration and its driving factors in the Beijing-Tianjin Sand Source Control

- Project Region, China. Agric. For. Meteorol. 200, 322–333. <https://doi.org/10.1016/j.agrformet.2014.10.008>.
- Sheffield, J., Wood, E.F., Pan, M., Beck, H., Coccia, G., Serrat-Capdevila, A., Verbist, K., 2018. Satellite remote sensing for water resources management: potential for supporting sustainable development in data-poor regions. Water Resour. Res. 54 (12), 9724–9758. <https://doi.org/10.1029/2017wr022437>.
- Shi, W.Y., Chen, Y.Z., Feng, X.M., 2020. Identifying the terrestrial carbon benefits from ecosystem restoration in ecologically fragile regions. Agric. Ecosyst. Environ. 296. <https://doi.org/10.1016/j.agee.2020.106889>.
- Sun, S.B., Song, Z.L., Wu, X.C., Wang, T.J., Wu, Y.T., Du, W.L., Che, T., Huang, C.L., Zhang, X.J., Ping, B., Lin, X.F., Li, P., Yang, Y.X., Chen, B.Z., 2018. Spatio-temporal variations in water use efficiency and its drivers in China over the last three decades. Ecol. Indic. 94, 292–304. <https://doi.org/10.1016/j.ecolind.2018.07.003>.
- Sun, S.K., Li, C., Wang, Y.B., Zhao, X.N., Wu, P.T., 2020. Evaluation of the mechanisms and performances of major satellite-based evapotranspiration models in Northwest China. Agric. For. Meteorol. 291. <https://doi.org/10.1016/j.agrformet.2020.108056>.
- Sun, X., Ren, G., Xu, W., Li, Q., Ren, Y., 2017. Global land-surface air temperature change based on the new CMA GLSAT data set. Sci. Bull. 62 (4), 236–238. <https://doi.org/10.1016/j.scib.2017.01.017>.
- Tan, X.J., Liu, B.J., Tan, X.Z., 2020. Global changes in baseflow under the impacts of changing climate and vegetation. Water Resour. Res. 56 (9). <https://doi.org/10.1029/2020wr027349>.
- Tao, F.L., Yokozawa, M., Xu, Y.L., Hayashi, Y., Zhang, Z., 2006. Climate changes and trends in phenology and yields of field crops in China, 1981–2000. Agric. For. Meteorol. 138 (1–4), 82–92. <https://doi.org/10.1016/j.agrformet.2006.03.014>.
- Tian, F., Lu, Y.H., Fu, B.J., Zhang, L., Zang, C.F., Yang, Y.H., Qiu, G.Y., 2017. Challenge of vegetation greening on water resources sustainability: insights from a modeling-based analysis in Northwest China. Hydrol. Process. 31 (7). <https://doi.org/10.1002/hyp.11118>.
- Tsai, Y., 2017. The multivariate climatic and anthropogenic elasticity of streamflow in the Eastern United States. J. Hydrol. Reg. Stud. 9, 199–215. <https://doi.org/10.1016/j.ejrh.2016.12.078>.
- Walker, E., Birch, J.B., 1988. Influence measures in ridge regression. Technometrics 30 (2), 221–227. <https://doi.org/10.2307/1270168>.
- Wang, J., Wang, K., Zhang, M., Zhang, C., 2015. Impacts of climate change and human activities on vegetation cover in hilly southern China. Ecol. Eng. 81, 451–461. <https://doi.org/10.1016/j.ecoleng.2015.04.022>.
- Wang, J., Xu, C., Hu, M., Li, Q., Jones, P., 2017. Global land surface air temperature dynamics since 1880. Int. J. Climatol. 11. <https://doi.org/10.1002/joc.5384>.
- Wang, Q.L., Wang, Y.P., Zhang, L., Qin, S.J., Zhang, Q., Liu, P., Liu, L., Zou, K.J., Cheng, S.J., Cheng, L., 2021a. Land surface models significantly underestimate the impact of land-use changes on global evapotranspiration. Environ. Res. Lett. 16 (12). <https://doi.org/10.1088/1748-9326/ac38db>.
- Wang, R., Li, L., Gentine, P., Zhang, Y., Chen, J., Chen, X., Chen, L., Ning, L., Yuan, L., Lu, G., 2022a. Recent increase in the observation-derived land evapotranspiration due to global warming. Environ. Res. Lett. 17 (2). <https://doi.org/10.1088/1748-9326/ac4291>.
- Wang, R., Li, L.H., Gentine, P., Zhang, Y., Chen, J.Y., Chen, X.W., Chen, L.J., Ning, L., Yuan, L.W., Lü, G.N., 2022b. Recent increase in the observation-derived land evapotranspiration due to global warming. Environ. Res. Lett. 17 (2), 10. <https://doi.org/10.1088/1748-9326/ac4291>.
- Wang, Y., Luo, W., Chen, J., Xianli, C., Zhang, L., Cheng, A., Wang, S., 2023. A dataset of carbon and water fluxes in the sample plots of natural regeneration at Puding Station of Guizhou Province (2015–2019). Chinese Scientific Data 8 (3). <https://doi.org/10.11922/11-6035.csd.2023.0063.zh>.
- Wang, Z.Z., Zhan, C.S., Ning, L.K., Guo, H., 2021b. Evaluation of global terrestrial evapotranspiration in CMIP6 models. Theor. Appl. Climatol. 143 (1–2), 521–531. <https://doi.org/10.1007/s00704-020-03437-4>.
- Wei, Y.Q., Lu, H.Y., Wang, J.N., Wang, X.F., Sun, J., 2022. Dual influence of climate change and anthropogenic activities on the spatiotemporal vegetation dynamics over the Qinghai-Tibetan Plateau from 1981 to 2015. Earths Future 10 (5), 23. <https://doi.org/10.1029/2021ef002566>.
- Xie, S.D., Mo, X.G., Hu, S., Liu, S.X., 2020. Contributions of climate change, elevated atmospheric CO₂ and human activities to ET and GPP trends in the Three-North Region of China. Agric. For. Meteorol. 295. <https://doi.org/10.1016/j.agrformet.2020.108183>.
- Yan, H., Yu, Q., Zhu, Z.C., Myneni, R.B., Yan, H.M., Wang, S.Q., Shugart, H.H., 2013. Diagnostic analysis of interannual variation of global land evapotranspiration over 1982–2011: assessing the impact of ENSO. J. Geophys. Res. Atmos. 118 (16), 8969–8983. <https://doi.org/10.1002/jgrd.50693>.
- Yan, W., Wang, H., Jiang, C., Jin, S., Ai, J., Sun, O.J., 2021. Satellite view of vegetation dynamics and drivers over southwestern China. Ecol. Indic. 130. <https://doi.org/10.1016/j.ecolind.2021.108074>.
- Yang, X., Li, Z., Feng, Q., He, Y., An, W., Zhang, W., Cao, W., Yu, T., Wang, Y., Theakstone, W.H., 2012. The decreasing wind speed in southwestern China during 1969–2009, and possible causes. Quat. Int. 263, 71–84. <https://doi.org/10.1016/j.quaint.2012.02.020>.
- Yao, Y.J., Liang, S.L., Li, X.L., Hong, Y., Fisher, J.B., Zhang, N.N., Chen, J.Q., Cheng, J., Zhao, S.H., Zhang, X.T., Jiang, B., Sun, L., Jia, K., Wang, K.C., Chen, Y., Mu, Q.Z., Feng, F., 2014. Bayesian multimodel estimation of global terrestrial latent heat flux from eddy covariance, meteorological, and satellite observations. J. Geophys. Res. Atmos. 119 (8), 4521–4545. <https://doi.org/10.1002/2013jd020864>.
- Yin, L.C., Tao, F.L., Zhai, R., Chen, Y., Hu, J., Wang, Z.H., Fu, B.J., 2022. Impacts of future climate change and atmospheric CO₂ concentration on ecosystem water retention service. Earths Future 10 (4), 23. <https://doi.org/10.1029/2021ef002138>.
- Ying, L.X., Kong, L.Q., Xiao, Y., Ouyang, Z.Y., 2022. The research progress and prospect of ecological security and its assessing approaches. Acta Ecol. Sin. 42 (5), 1679–1692. <https://doi.org/10.5846/stxb202104171002>.
- Yu, D.Y., Li, X.Y., Cao, Q., Hao, R.F., Qiao, J.M., 2020. Impacts of climate variability and landscape pattern change on evapotranspiration in a grassland landscape mosaic. Hydrol. Process. 34 (4), 1035–1051. <https://doi.org/10.1002/hyp.13642>.
- Zhang, D., Liu, X., Zhang, L., Zhang, Q., Gan, R., Li, X., 2020. Attribution of evapotranspiration changes in humid regions of China from 1982 to 2016. J. Geophys. Res. Atmos. 125 (13). <https://doi.org/10.1029/2020jd032404>.
- Zhang, J., Chen, H.-S., Nie, Y.-P., Fu, Z.-Y., Lian, J.-J., Wang, F., Luo, Z.-D., Wang, K.-L., 2024. Research progress on structure and hydrological processes in the karst critical zone of southwest China. J. Appl. Ecol. 35 (4), 985–996. <https://doi.org/10.13287/j.1001-9332.202404.020>.
- Zhang, K., Kimball, J.S., Running, S.W., 2016a. A review of remote sensing based actual evapotranspiration estimation. Wiley Interdiscip. Rev. Water 3 (6), 834–853. <https://doi.org/10.1002/wat2.1168>.
- Zhang, P.P., Cai, Y.P., He, Y.H., Xie, Y.L., Zhang, X.D., Li, Z., 2022. Changes of vegetational cover and the induced impacts on hydrological processes under climate change for a high-diversity watershed of south China. J. Environ. Manag. 322, 11. <https://doi.org/10.1016/j.jenvman.2022.115963>.
- Zhang, Q., Yang, Z., Hao, X., Yue, P., 2019. Conversion features of evapotranspiration responding to climate warming in transitional climate regions in northern China. Clim. Dyn. 52 (7–8), 3891–3903. <https://doi.org/10.1007/s00382-018-4364-3>.
- Zhang, Y.Q., Pena-Arancibia, J.L., McVicar, T.R., Chiew, F.H.S., Vaze, J., Liu, C.M., Lu, X. J., Zheng, H.X., Wang, Y.P., Liu, Y.Y., Miralles, D.G., Pan, M., 2016b. Multi-decadal trends in global terrestrial evapotranspiration and its components. Sci. Rep. 6, 12. <https://doi.org/10.1038/srep19124>.
- Zhang, Y.Q., You, Q.L., Ullah, S., Chen, C.C., Shen, L.C., Liu, Z., 2023a. Substantial increase in abrupt shifts between drought and flood events in China based on observations and model simulations. Sci. Total Environ. 876. <https://doi.org/10.1016/j.scitotenv.2023.162822>.
- Zhang, Z., Hu, B.Q., Jiang, W.G., Qiu, H.H., 2023b. Construction of ecological security pattern based on ecological carrying capacity assessment 1990–2040: a case study of the Southwest Guangxi Karst-Beibu Gulf. Ecol. Model. 479. <https://doi.org/10.1016/j.ecolmodel.2023.110322>.
- Zhang, Z., Hu, B.Q., Qiu, H.H., 2021. Comprehensive assessment of ecological risk in southwest Guangxi-Beibu bay based on DPSIR model and OWA-GIS. Ecol. Indic. 132. <https://doi.org/10.1016/j.ecolind.2021.108334>.
- Zhao, F.B., Ma, S., Wu, Y.P., Qiu, L.J., Wang, W.K., Lian, Y.Q., Chen, J., Sivakumar, B., 2022. The role of climate change and vegetation greening on evapotranspiration variation in the Yellow River Basin, China. Agric. For. Meteorol. 316, 14. <https://doi.org/10.1016/j.agrformet.2022.108842>.
- Zhao, M.S., Running, S.W., 2010. Drought-induced reduction in global terrestrial net primary production from 2000 through 2009. Science 329 (5994), 940–943. <https://doi.org/10.1126/science.1192666>.
- Zheng, H., Miao, C., Li, X., Kong, D., Gou, J., Wu, J., Zhang, S., 2022. Effects of vegetation changes and multiple environmental factors on evapotranspiration across China over the past 34 years. Earth Fut. 10 (4). <https://doi.org/10.1029/2021ef002564>.
- Zheng, H.X., Zhang, L., Zhu, R.R., Liu, C.M., Sato, Y., Fukushima, Y., 2009. Responses of streamflow to climate and land surface change in the headwaters of the Yellow River Basin. Water Resour. Res. 45. <https://doi.org/10.1029/2007wr006665>.
- Zhu, G.F., Su, Y.H., Li, X., Zhang, K., Li, C.B., Ning, N., 2014. Modelling evapotranspiration in an alpine grassland ecosystem on Qinghai-Tibetan plateau. Hydrol. Process. 28 (3), 610–619. <https://doi.org/10.1002/hyp.9597>.